

Synthesis and structure of two-dimensional transition-metal dichalcogenides

Yumeng Shi, Hua Zhang, Wen-Hao Chang, Hyeon Suk Shin, and Lain-Jong Li

Two-dimensional (2D) transition-metal dichalcogenides (TMDCs) exhibit unique electrical, optical, thermal, and mechanical properties, which enable them to be used as building blocks in compact and lightweight integrated electronic systems. The controllable and reliable synthesis of atomically thin TMDCs is essential for their practical application. Recent progress in large-area synthesis of monolayer TMDCs paves the way for practical production of various 2D TMDC layers. The intrinsic optical and electrical properties of monolayer TMDCs can be defined by stoichiometry during synthesis. By manipulating the lattice structure or layer stacking manner, it is possible to create atomically thin van der Waals materials with unique and unexplored physical properties. In this article, we review recent developments in the synthesis of TMDC monolayers, alloys, and heterostructures, which shine light on the design of novel TMDCs with desired functional properties.

Structure of transition-metal dichalcogenides

Atomically thin transition-metal dichalcogenides (TMDCs) provide a wide range of unique electrical, optical, and thermal properties that do not exist in their bulk counterparts (see the Introductory article in this issue of *MRS Bulletin*).^{1,2} Monolayer molybdenum disulfide (MoS_2),³ one of the most important and frequently studied TMDCs, exhibits good chemical stability and mechanical flexibility. Meanwhile, its semiconducting nature provides a high ON/OFF current ratio in transistors, and TMDC monolayers (MoS_2 , WS_2 , MoSe_2 , and WSe_2) with a direct bandgap give strong bandgap emission.⁴⁻⁶ With large carrier mobility and good mechanical properties, two-dimensional (2D) TMDCs are considered as promising candidates for wearable and flexible systems.^{4,7}

Other TMDC materials, such as molybdenum diselenide (MoSe_2), tungsten disulfide (WS_2), and tungsten diselenide (WSe_2), have also attracted much recent attention.^{8,9} Being an inorganic graphite analogue, all TMDCs share a similar material structure. Each TMDC layer has a sandwich structure formed by hexagonally packed transition-metal atoms located between two layers of chalcogen atoms. Similar to graphite,

a weak van der Waals (vdW) force holds each TMDC layer together; thus, the bulk crystal can be exfoliated along the 2D surface.

Three main polytypes

In a TMDC monolayer, the transition-metal and chalcogen atoms form strong covalent bonds, giving rise to several stacking polytypes and polymorphs. The commonly found structural polytypes of TMDC are 1T, 2H, and 3R, which refer to one (1), two (2), and three (3) layers per unit cell stacking in the tetragonal (T), hexagonal (H), and rhombohedral (R) symmetry, respectively. Considering MoS_2 as an example, all three polytypes of MoS_2 have regular layered structures with six-fold trigonal prismatic coordination of transition-metal atoms (Mo) surrounded by chalcogen atoms (S).¹⁰ One tetragonal- MoS_2 is a metastable metallic phase, while 2H- MoS_2 and 3R- MoS_2 are thermodynamically stable phases that can be found in nature. One tetragonal- and 2H- MoS_2 differ only by a transversal displacement of one of the two sulfur planes. As shown in **Figure 1a**, it has been suggested that lithium-ion intercalation results in the 2H to 1T phase transformation.¹¹ Since the 1T structure is typically unstable, a 1T' structure can

Yumeng Shi, Physical Sciences and Engineering, King Abdullah University of Science and Technology, Saudi Arabia; yumeng.shi@kaust.edu.sa

Hua Zhang, School of Materials Science and Engineering, Nanyang Technological University, Singapore; hzhang@ntu.edu.sg

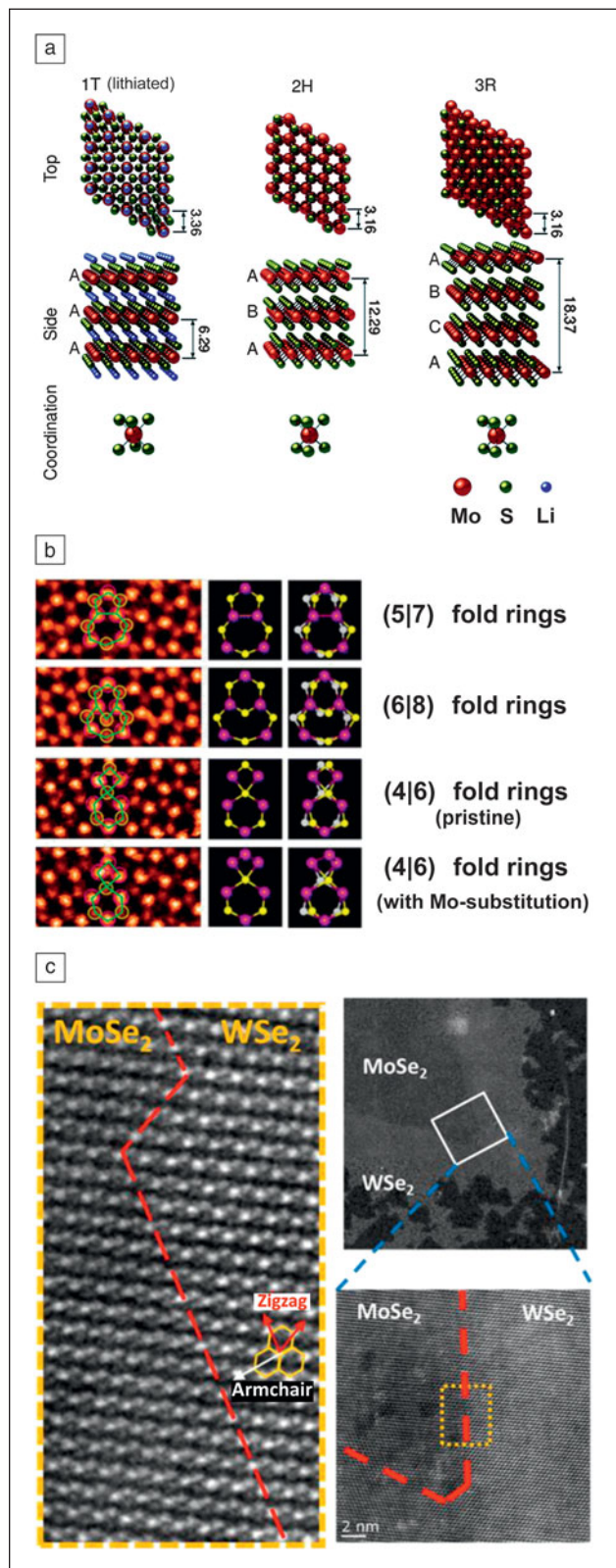
Wen-Hao Chang, Department of Electrophysics, National Chiao Tung University, Taiwan; whchang@mail.nctu.edu.tw

Hyeon Suk Shin, Department of Chemistry and Department of Energy Engineering, Ulsan National Institute of Science and Technology, South Korea; shin@unist.ac.kr

Lain-Jong Li, King Abdullah University of Science and Technology, Saudi Arabia; lance.li@kaust.edu.sa

DOI: 10.1557/mrs.2015.121

also form by a spontaneous lattice distortion.^{12,13} On the other hand, the incorporation of impurity elements, such as Re and Nb in the MoS₂ layers, leads to a partial substitution of the Mo atoms and results in more stable 3R packing.



Interfacing and quantum confinement in 2D materials

Because of a large aspect ratio, the interfacing and quantum confinement in 2D materials are commonly intertwined and thus, determine their electronic and/or optical properties.¹⁴ Both computational and experimental results have confirmed that the coupling between electronic transitions and phonons are significantly improved when MoS₂ is scaled down from three-dimensional to 2D geometry. For example, bulk MoS₂ is an indirect bandgap semiconductor with very weak photoluminescence (PL).¹⁵ Surprisingly, when the MoS₂ layers are thinned down to just a few or to a monolayer thickness, the PL becomes significant.¹⁵ The striking contrast in PL emission between bulk and monolayer MoS₂ originally arises from the quantum confinement in layered *d*-electron materials, where the characteristics of the *d*-electron orbitals comprise the conduction and valence bands. Therefore, the emergence of strong PL in monolayer TMDCs and indirect to direct bandgap conversion have also been observed in other layered TMDCs such as MoSe₂, WS₂, and WSe₂.^{2,8,9}

Grain boundary and edge reconstruction

The mechanical, electronic, optical, and chemical properties of TMDC materials strongly depend on their structure. Intrinsic point defects, dislocations, grain boundaries, and type of edges in TMDC layers have been experimentally identified.^{16–19} MoS₂ growth has been shown to follow a layer-plus-island (or Stranski–Krastanov) growth mode,^{8,20} where monolayer MoS₂ domains initially gather and interconnect with each other until the full coverage of the monolayer is complete.²⁰ Najmaei et al. have demonstrated that coalescence of TMDC grains leads to the formation of grain boundaries with arrays of dislocations of pristine and sulfur-substituted (5|7) fold rings,¹⁹ where (5|7) means that dislocations consist of 5 and 7 atom ring structures folded together. Furthermore, a rich variety of point defects and dislocation cores have been identified in MoS₂ layers using aberration-corrected scanning transmission electron microscope (STEM). Figure 1b shows the core structures of (5|7), (6|8), and (4|6), and other core structures such as (4|6) and (4|8) fold rings, which have also been identified by Zhou et al.¹⁷

Figure 1. Structure of transition-metal dichalcogenides (TMDCs). (a) Three main structural polytypes identified as one tetragonal (1T)-MoS₂, two hexagonal (2H)-MoS₂, and three rhombohedral (3R)-MoS₂. (b) Scanning tunneling microscopy images showing the structure with (5|7) fold rings and new core structures with (4|4), (4|6), (4|8), and (6|8) fold rings. The yellow white and purple spheres represent top and bottom S and Mo, respectively. (c) High resolution high-angle annular dark-field scanning transmission electron microscopy image of MoSe₂/WSe₂ heterostructures. The image in the yellow dotted box is a close-up of the region highlighted on the right. (left) The close-up shows the in-plane lateral heteroepitaxial growth of the TMDC materials results in well-defined lateral heterostructures of MoSe₂/WSe₂ with an atomically abrupt lateral interface, as indicated by the red dashed line in the left micrograph. (a) Reproduced with permission from Reference 10. © 2014 Royal Society of Chemistry. (b) Reproduced with permission from Reference 17. © 2013 American Chemical Society. (c) Reproduced with permission from Reference 21. © 2014 American Chemical Society.

Monolayer MoS₂ has a direct bandgap with strong PL. PL mapping can also be used to distinguish the grain boundary from pristine TMDC regions. Since the reconstruction of atoms along the grain boundaries may generate new states near the Fermi level, a locally modified PL emission around the junction of different grains is typically observed. Van der Zande et al. used PL mapping to image the grain boundaries of polycrystalline TMDC monolayers.¹⁸ Significant differences in PL intensity and peak shift have also been observed from polycrystalline MoS₂ with mirror symmetric and faceted tilt grain boundaries. The mirror boundary shows an 8 meV upshift in peak energy and a decrease in peak intensity, while the tilted boundary shows enhanced PL emission and a 26 meV upshift in peak energy.¹⁸

Additionally, TMDC materials can also form in-plane heterostructures, which lead to interesting edge reconstruction of atoms along the TMDC heterojunctions. As shown in Figure 1c, in-plane lateral heteroepitaxial growth of TMDCs has recently been realized. Well-defined lateral WS₂/MoS₂ heterostructures were synthesized via chemical vapor deposition (CVD) and further demonstrated the ability to form an intrinsic monolayer *p-n* junction.²¹ Gong et al. have fabricated an atomically abrupt lateral interface between MoS₂ and WS₂ with atomic precision.²² An atomically coherent lateral interface between WS₂ and MoS₂ appears as a straight line and preferentially along the zigzag direction, with occasionally observed lateral junctions along the armchair direction. Transition-metal elements are found to diffuse over a width of 1–3 unit cells around the armchair interfaces, which is likely due to the relatively low stability of armchair edges during epitaxial growth.

Duane et al. has also reported nearly coherent heterostructure between WS₂ and WSe₂.²³ However, energy dispersive x-ray spectroscopy line scan profiles suggest there is no atomically abrupt junction formation, and the WS₂ to WSe₂ phase transition typically exists over a length range of ~35 nm. This gradual interface was attributed to the slow switching of vapor-phase reactants during growth. Zhang et al. have also demonstrated direct synthesis of lateral MoS₂/WS₂ and MoSe₂/WSe₂ heterostructures.²¹ Atomic-resolution STEM has revealed that the lateral heterostructure picks the zigzag direction of the lattice instead of the armchair direction. Note that an abrupt heterojunction may present interesting interlayer excitonic features and distinct *p-n* junction properties.

Chemical exfoliation of TMDCs

The mechanical cleavage technique, first used to produce graphene in 2004,²⁴ is the typical exfoliation method to prepare monolayers and multilayers from their bulk crystals.^{25–29} Although pristine, large-size, single-layer TMDC nanosheets can be obtained by mechanical cleavage, its low throughput has limited practical applications. Alternatively, chemical exfoliation has been developed to realize high-yield and large-scale production of TMDC nanosheets in solution phase.

In this section, we focus on various kinds of chemical exfoliation approaches for TMDC nanosheets, with an emphasis on the advantages and disadvantages of each method.

Direct sonication in common solvents or polymer aqueous solutions

As a typical example, Coleman and co-workers demonstrated that bulk TMDC crystals can be effectively exfoliated by direct sonication in common solvents (e.g., *N*-methyl-pyrrolidone [NMP] and dimethylformamide [DMF]).²⁹ A number of single or a few-layer TMDC nanosheets, such as MoS₂, WS₂, MoSe₂, NbSe₂, TaSe₂, NiTe₂, and MoTe₂, were prepared from their bulk crystals using this method. Both theoretical calculation and experimental results revealed that the degree to which the surface energies match between the solvent and the layered crystal can be used to minimize the enthalpy of exfoliation and is a key factor for achieving effective exfoliation. For example, in the case of exfoliation of MoS₂, NMP is the most effective solvent whose surface tension matches well with the surface energy of MoS₂.

Typically, solvents with surface tensions close to 40 mJ/m² are required to exfoliate most layered compounds.^{29–32} Unfortunately, it was found that water, the most commonly used solvent, has a surface tension of 72 mJ/m², which is not suitable for exfoliation of TMDC sheets. Intriguingly, Zhang and co-workers reported that a water–ethanol mixture is suitable to exfoliate and disperse 2D TMDC nanosheets by sonication, although individually, neither water nor ethanol has proved to be a suitable solvent for the exfoliation of TMDC crystals.³⁰ This obvious difference is attributed to the change in solubility parameters upon mixing of the solvents. This method is convenient, economical, and potentially scalable since water and ethanol are commonly used solvents.

Coleman and co-workers also reported on the exfoliation of TMDC crystals by sonication in a polymer aqueous solution.³¹ They found that a number of layered crystals can be exfoliated in water in the presence of a polymer, resulting in well-dispersed TMDC nanosheets coated with the polymer. Large-scale production of 2D TMDC nanosheets can be achieved by direct exfoliation or polymer-assisted methods.³² Due to limitations of the sonication process, however, the yield of single-layer sheets produced by these methods is relatively low, and the lateral size of the sheets is relatively small and non-uniform (from several nm to several hundred μm range).³² Moreover, the polymers coated on the TMDC nanosheets are undesirable for some applications.³¹

Ion intercalation and exfoliation

The intercalation of layered TMDC crystals with *n*-butyllithium in hexane followed by exfoliation in water via sonication was developed in the 1970s to produce single-layer TMDC nanosheets.^{33–36} In this process, the lithium (Li) ions were intercalated into the layered spacing, and they reacted with the TMDC crystals to form Li-intercalated compounds (e.g., for MoS₂, the compound is Li_{*x*}MoS₂, where *x* is the number of Li atoms).^{33,34}

The Li-intercalated compounds were then sonicated in water or ethanol to obtain well-dispersed single-layer sheets.

Note that the H_2 gas generated from the reaction between lithium and water (or ethanol) also helps to further push the stacked TMDC layers apart. Based on this method, a range of well-dispersed TMDC monolayers, such as MoS_2 , WS_2 , and TiS_2 , have been prepared in high-yield and large amounts. It is worth pointing out that the yield of single layers obtained by this method is much higher than that using the direct sonication or sonication in polymer aqueous solution. A unique advantage of this method is the phase transformation from the 2H to the 1T phase of some TMDC nanosheets (e.g., MoS_2 and WS_2) during the interaction process. This offers great opportunities to realize superior performance for specific applications (e.g., electrocatalysis and transistors) via phase engineering.^{37,38}

Recently, Loh and co-workers reported a modified method to produce TMDC sheets with large size. First, bulk TMDC crystals were expanded with hydrazine (N_2H_4) by the hydrothermal method.⁸⁴ Sodium naphthalenide rather than *n*-butyllithium was used as the intercalation agent. By using their method, a variety of TMDC sheets, such as MoS_2 , TiS_2 , TaS_2 , and WS_2 , with lateral sizes up to tens of micrometers, were obtained. However, the intercalation process needs high temperatures (e.g., $100^\circ C$) and long reaction times (e.g., three days). Moreover, uncontrollable lithium/sodium intercalation leads to incomplete lithium intercalation or over-insertion of lithium, resulting in either a low yield of single layers or decomposition of TMDC nanosheets into metal nanoparticles and Li_2S .

Recently, Zhang developed an electrochemical Li-intercalation and exfoliation method to produce various TMDC nanosheets (Figure 2a), including MoS_2 , WS_2 , TiS_2 , TaS_2 , ZrS_2 , and $NbSe_2$.^{39–41} The layered bulk crystals were integrated in a Li-ion battery cell as the cathode, and a lithium foil was used as an anode. The Li interaction process was conducted during the discharge process. Based on this method, a series of single or few-layer TMDC nanosheets, such as MoS_2 , TiS_2 , TaS_2 , and WS_2 (Figure 2b), could be prepared with high yield and at a large scale, in which the yield of single-layer MoS_2 and TaS_2 sheets reached over 90%. In contrast to intercalation with organometallic compounds, this electrochemical Li-intercalation method can be easily carried out at room temperature in less than six hours. Importantly, the Li-intercalation process could be well controlled by monitoring the discharge curve to avoid insufficient Li intercalation or over Li insertion.

Vapor phase deposition of TMDCs

The synthesis of uniform and large-area TMDC layers is an essential requirement for their practical application in electronic and optical devices.^{8,9} Vapor phase deposition, a bottom-up synthesis strategy, provides a synthetic route that can be employed to obtain monolayer TMDCs, heterostructure alloys, and multilayer stackings. It shows great promise to generate high-quality TMDC layers with scalable size, controllable thickness, and excellent electronic properties.

Vapor phase reaction for monolayer TMDC growth

As shown in Figure 3, there have been attempts to produce TMDC layers via sulfurization of a transition-metal or metal

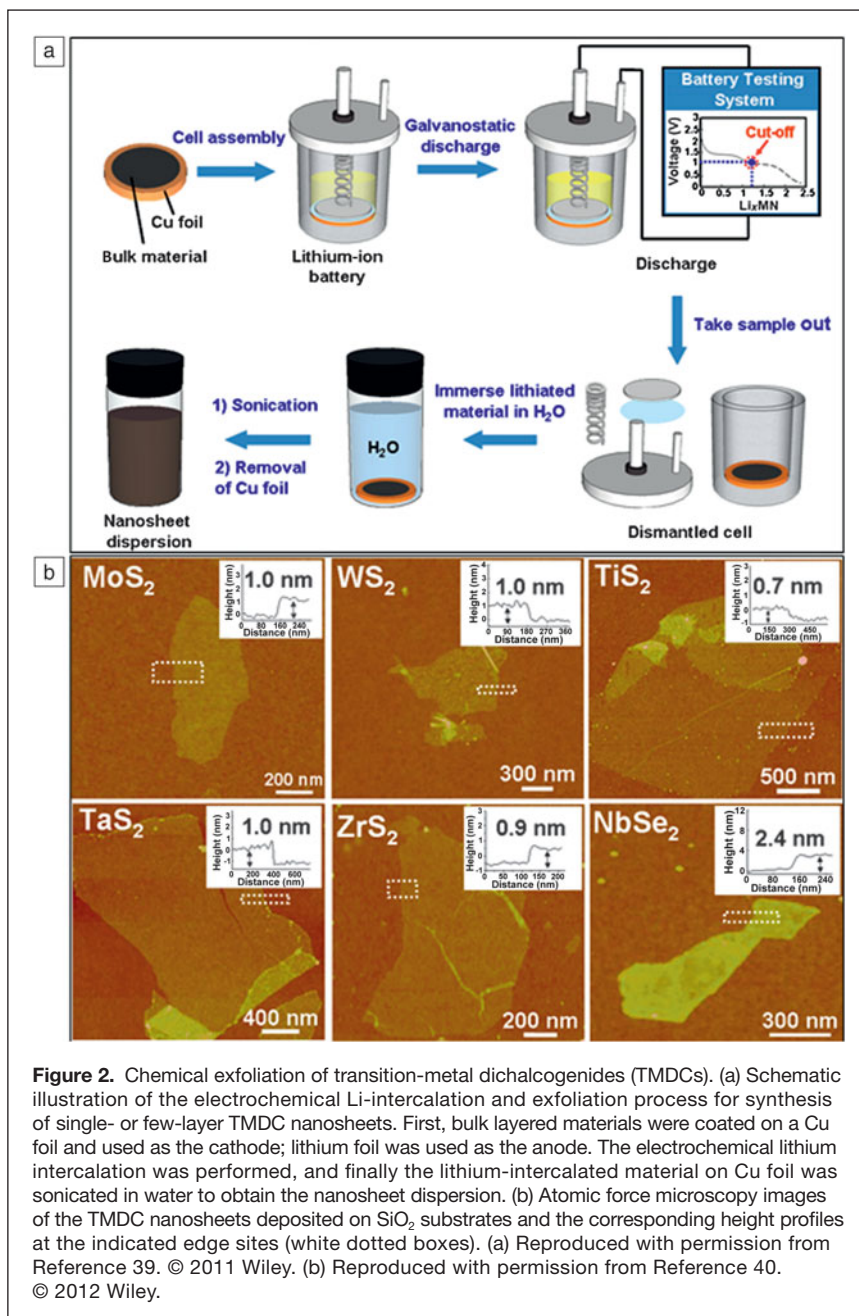
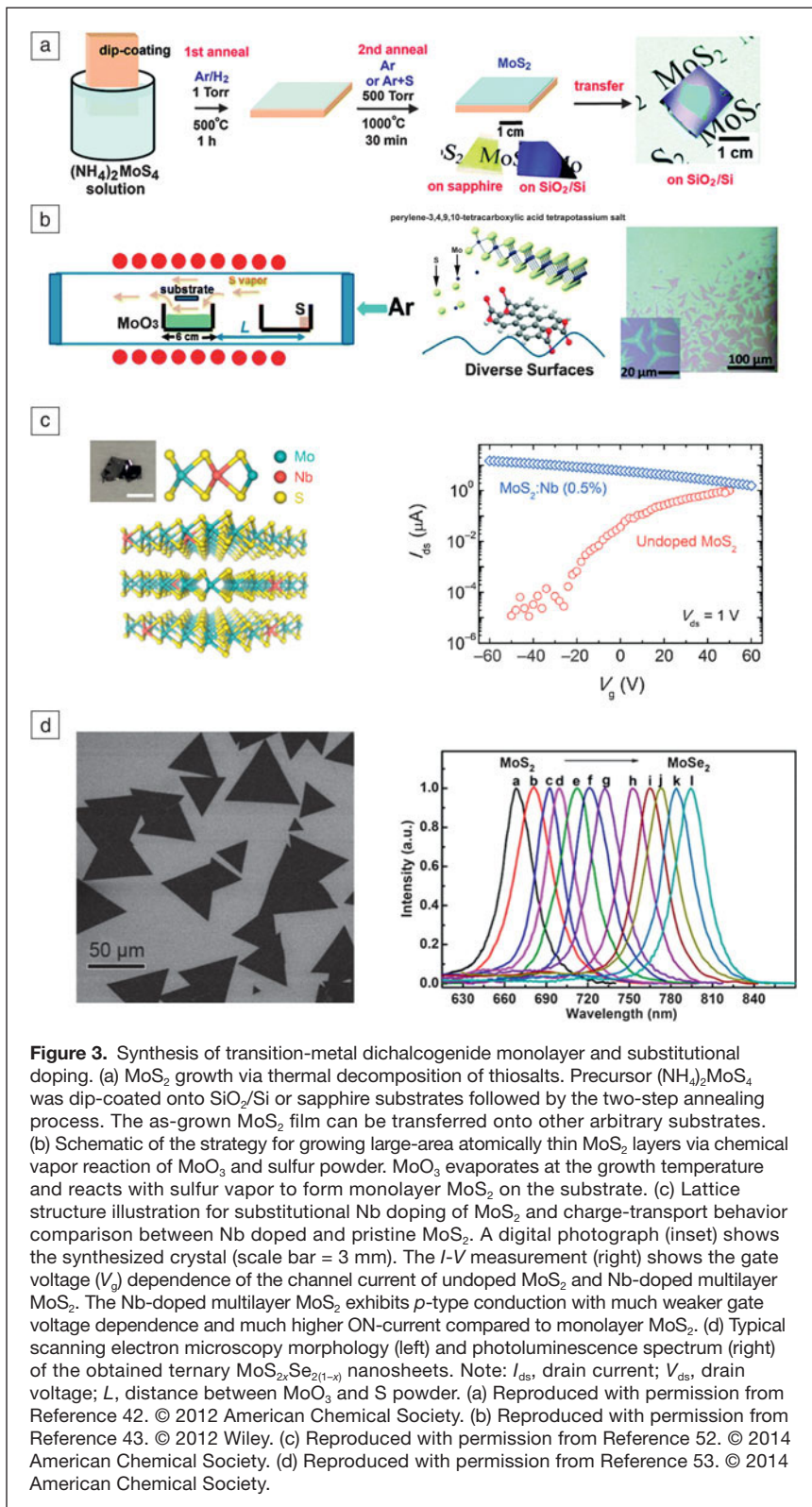


Figure 2. Chemical exfoliation of transition-metal dichalcogenides (TMDCs). (a) Schematic illustration of the electrochemical Li-intercalation and exfoliation process for synthesis of single- or few-layer TMDC nanosheets. First, bulk layered materials were coated on a Cu foil and used as the cathode; lithium foil was used as the anode. The electrochemical lithium intercalation was performed, and finally the lithium-intercalated material on Cu foil was sonicated in water to obtain the nanosheet dispersion. (b) Atomic force microscopy images of the TMDC nanosheets deposited on SiO_2 substrates and the corresponding height profiles at the indicated edge sites (white dotted boxes). (a) Reproduced with permission from Reference 39. © 2011 Wiley. (b) Reproduced with permission from Reference 40. © 2012 Wiley.



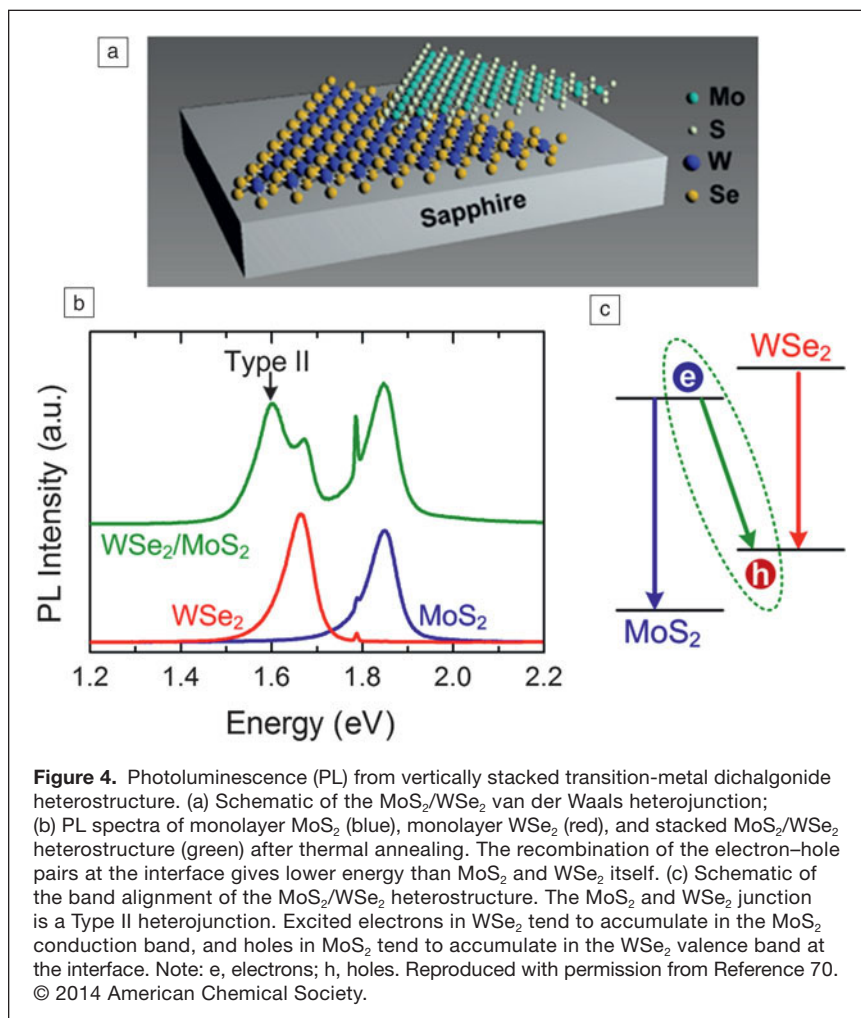
oxide thin film, thermal decomposition of thioaltes,⁴² and vapor phase transport of TMDC powders.⁹ However, it remains a challenge to obtain a high-quality TMDC with a desired number of layers, since the thickness of the precursor coating

or the amount of reactant needs to be precisely controlled. Li et al. have reported a strategy for growing large-area atomically thin MoS₂ layers via chemical vapor reaction of MoO₃ and sulfur powder (Figure 3b).⁴³ During TMDC growth, the transition-metal oxide in the vapor phase undergoes a two-step reaction, where a suboxide compound likely forms during the reaction, which serves as an intermediate that diffuses to the substrate and further reacts with sulfur vapors to grow TMDC layers.

It is anticipated that the surface energy control of the growth substrate is critical for the nucleation and crystallization of TMDC layers.^{43,44} The presence of aromatic molecules has been shown to provide better wetting between precursors and the substrate surface to promote TMDC nucleation.⁴⁴ Van der Zande et al. have reported a refined chemical vapor reaction route for ultra-large MoS₂ synthesis.¹⁸ The growth of the TMDC layer was found to be sensitive to the properties of the substrate surfaces. By using clean substrates and fresh precursors, ultra-large MoS₂ crystalline islands with an average size between 20 μm and 100 μm were obtained. Najmaei et al. found MoS₂ crystals with triangular shapes commonly nucleate and form on the step edges.¹⁹ Therefore, it is possible to control the growth location of MoS₂ layers by patterning the substrates using conventional lithography processes. The patterns on the growth substrate can significantly reduce the nucleation energy barrier of MoS₂, thus realizing the synthesis of TMDC layers at predefined locations. Eichfeld et al. have demonstrated a highly scalable synthesis approach of large-area WSe₂ (yielding >8 μm size domains) via metal-organic CVD (MOCVD) using tungsten hexacarbonyl (W(CO)₆) and dimethylselenium ((CH₃)₂Se) as growth precursors.⁴⁵ The MOCVD method allows for excellent control over the process conditions, which is critical for large-scale, high-quality TMDC production.

The direct vapor phase reaction of transition-metal oxide and sulfur/selenium has been widely applied by many research groups to produce TMDC layers such as MoS₂, WS₂, MoSe₂, and WSe₂.^{8,9} The vapor phase reaction method allows the growth of single-crystalline TMDC flakes directly on arbitrary substrates

without the need for an additional transfer process for electronic device fabrication. It has become a widely adopted approach for producing TMDC monolayers for electrical property studies.



Substitutional doping of TMDC layers for bipolar transport

Both *n*- and *p*-type TMDC-based field-effect transistors are required in order to integrate them in low-power consumption, high-performance, complementary logic circuits. Meanwhile, bipolar carrier conduction is also essential for TMDC-based optoelectronic devices, such as light-emitting diodes and photodetectors, which require electron-hole pair generation and recombination. MoS₂ has been widely accepted as an *n*-type semiconductor due to omnipresent sulfur vacancies.⁴⁶

Although *p*-type doping for TMDCs can be achieved by surface adsorption⁴⁷ or intercalation of electron accepting molecules,^{48–50} substitutional doping is considered a more practical and stable approach since the dopant is secured by covalent bonding. Density functional theory has been used to study possible substitutional doping strategies for MoS₂ monolayers,⁵¹ where the replacement of Mo by Nb is the most promising *p*-doping method.

Experimentally, Suh and co-workers have demonstrated that Nb doping in the MoS₂ layer leads to stable *p*-type conduction, as shown in Figure 3c.⁵² The Nb-doped MoS₂ crystals with a nominal 0.5% Nb doping were grown by a chemical

vapor transport method, where iodine was used as the transport agent. However, this method could only produce MoS₂:Nb bulk crystals, which need further exfoliation to obtain atomically thin-layered 2D materials for electronic device fabrication. The MoS₂:Nb device exhibits *p*-type conduction, but the gate voltage (V_g) dependence becomes much weaker, which can be attributed to the degeneracy of the Nb doping level.

TMDC ternary van der Waals alloys

The intrinsic bandgap of TMDCs can be engineered by their stoichiometry. Recently, both Mo_{1-x}W_xS₂ and MoS_{2-x}Se_{2(1-x)} ($x = 0 - 1$) alloys have been synthesized via CVD.^{53–55} As shown in Figure 3d, the successful synthesis of TMDC alloys provides a versatile change in their band structure, and a tunable bandgap emission has been observed.

Additionally, being an important 2D diluted magnetic semiconductor, Co-doped MoS₂ has recently been investigated both theoretically and experimentally.⁵⁶ Li et al. reported the synthesis of large-scale Co_xMo_{1-x}S₂ ($x = 0.16$) nanosheets by an adapted CVD method,⁵⁶ where Co₃O₄ and MoO₃ powder were used as precursors, and sulfur was placed at a hot zone to generate sulfur vapor for the growth. The Co_xMo_{1-x}S₂ nanosheets exhibit *n*-type semiconducting transport behavior. Interestingly, when the growth temperature is increased from 680°C to 750°C, CoS₂ gradually grows on the surface of Co_xMo_{1-x}S₂ following the shape of the underlying 2D layers.

Synthesis of artificial TMDC heterostructures

vdW layered materials have strong in-plane bonding and weak vdW interplanar interactions. Combining the unique properties of different 2D layered materials, including graphene, h-BN, and TMDCs, into hybrid vdW heterostructures offers the possibility to create novel 2D building blocks with new functionalities for versatile applications.⁵⁷ The success of vdW hybrid materials is manifested in flexible photovoltaic devices^{58,59} and field-effect tunneling transistors.⁶⁰ MoS₂/graphene or graphene/MoS₂ heterostructures also have shown great potential in many novel applications, such as electronic logic and memory devices,⁷ ultrasensitive detection of deoxyribonucleic acid (DNA) hybridization,⁶¹ hydrogen evolution reaction,^{62,63} and energy storage.^{64,65}

On the other hand, considerable effort has been made in creating heterostructures formed by different 2D semiconducting TMDCs. The main theme originates from the heterostructures of conventional Group IV or III–V semiconductors with different bandgaps, which already lie at

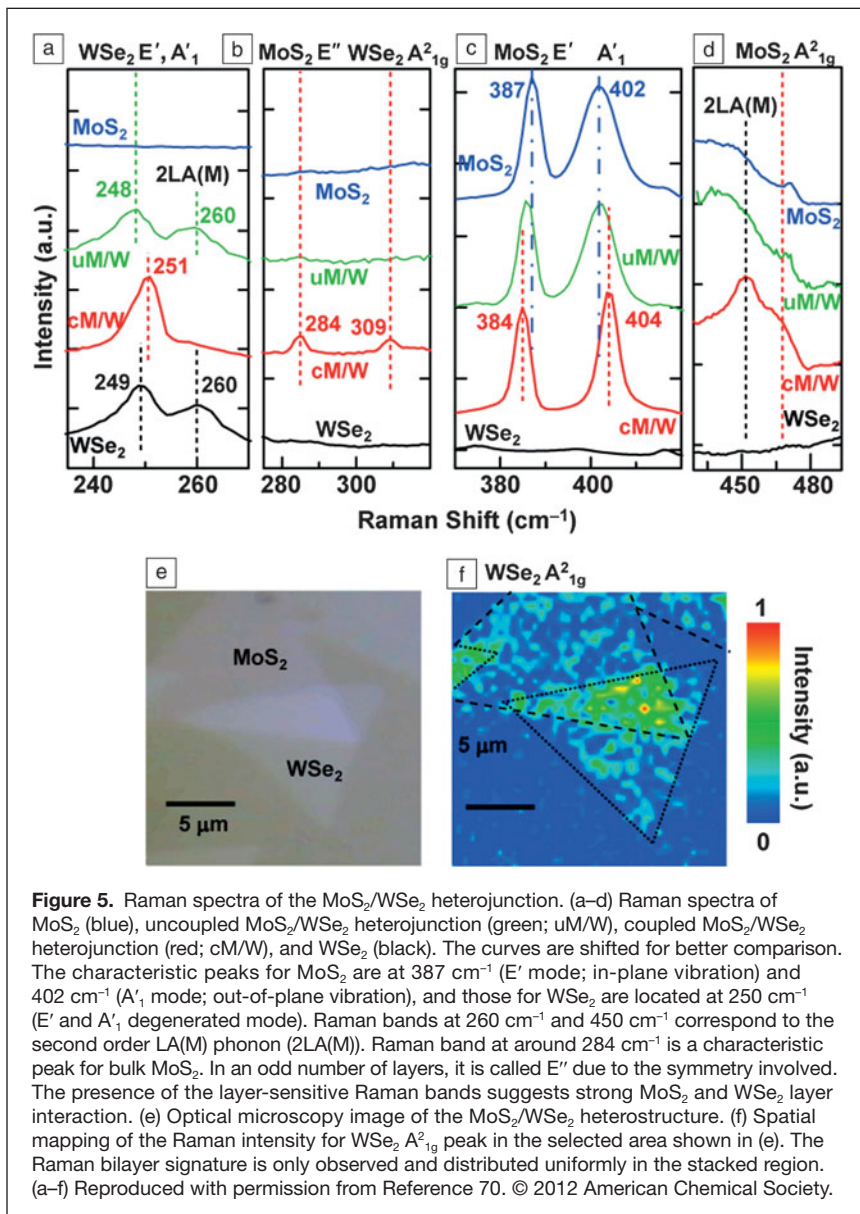


Figure 5. Raman spectra of the MoS₂/WSe₂ heterojunction. (a–d) Raman spectra of MoS₂ (blue), uncoupled MoS₂/WSe₂ heterojunction (green; uM/W), coupled MoS₂/WSe₂ heterojunction (red; cM/W), and WSe₂ (black). The curves are shifted for better comparison. The characteristic peaks for MoS₂ are at 387 cm⁻¹ (E' mode; in-plane vibration) and 402 cm⁻¹ (A₁' mode; out-of-plane vibration), and those for WSe₂ are located at 250 cm⁻¹ (E' and A₁', degenerated mode). Raman bands at 260 cm⁻¹ and 450 cm⁻¹ correspond to the second order LA(M) phonon (2LA(M)). Raman band at around 284 cm⁻¹ is a characteristic peak for bulk MoS₂. In an odd number of layers, it is called E'' due to the symmetry involved. The presence of the layer-sensitive Raman bands suggests strong MoS₂ and WSe₂ layer interaction. (e) Optical microscopy image of the MoS₂/WSe₂ heterostructure. (f) Spatial mapping of the Raman intensity for WSe₂ A_{21g} peak in the selected area shown in (e). The Raman bilayer signature is only observed and distributed uniformly in the stacked region. (a–f) Reproduced with permission from Reference 70. © 2012 American Chemical Society.

the heart of modern semiconductor electronics and optoelectronics. Layer-by-layer stacking of TMDCs with different bandgaps thus represents a 2D analogue, which opens up opportunities for engineering material properties for device applications. For example, by combining *n*-type MoS₂ and *p*-type WSe₂ monolayers, it is possible to realize atomically thin vdW *p*–*n* junctions. Artificial stacking through “peel-and-paste” processes (i.e., mechanical transfer of one TMDC monolayer onto another) is the most straightforward method to construct TMDC heterostructures.

Theoretical studies based on first-principles *ab initio* calculations suggest that the MoX₂/WX₂ (X = S, Se) heterostructure exhibits a Type II semiconductor heterojunction with a staggered bandgap alignment.^{66–68} Observation of the interlayer Type II optical transition is a fingerprint of interlayer coupling between two dissimilar TMDC monolayers. Indeed, PL from

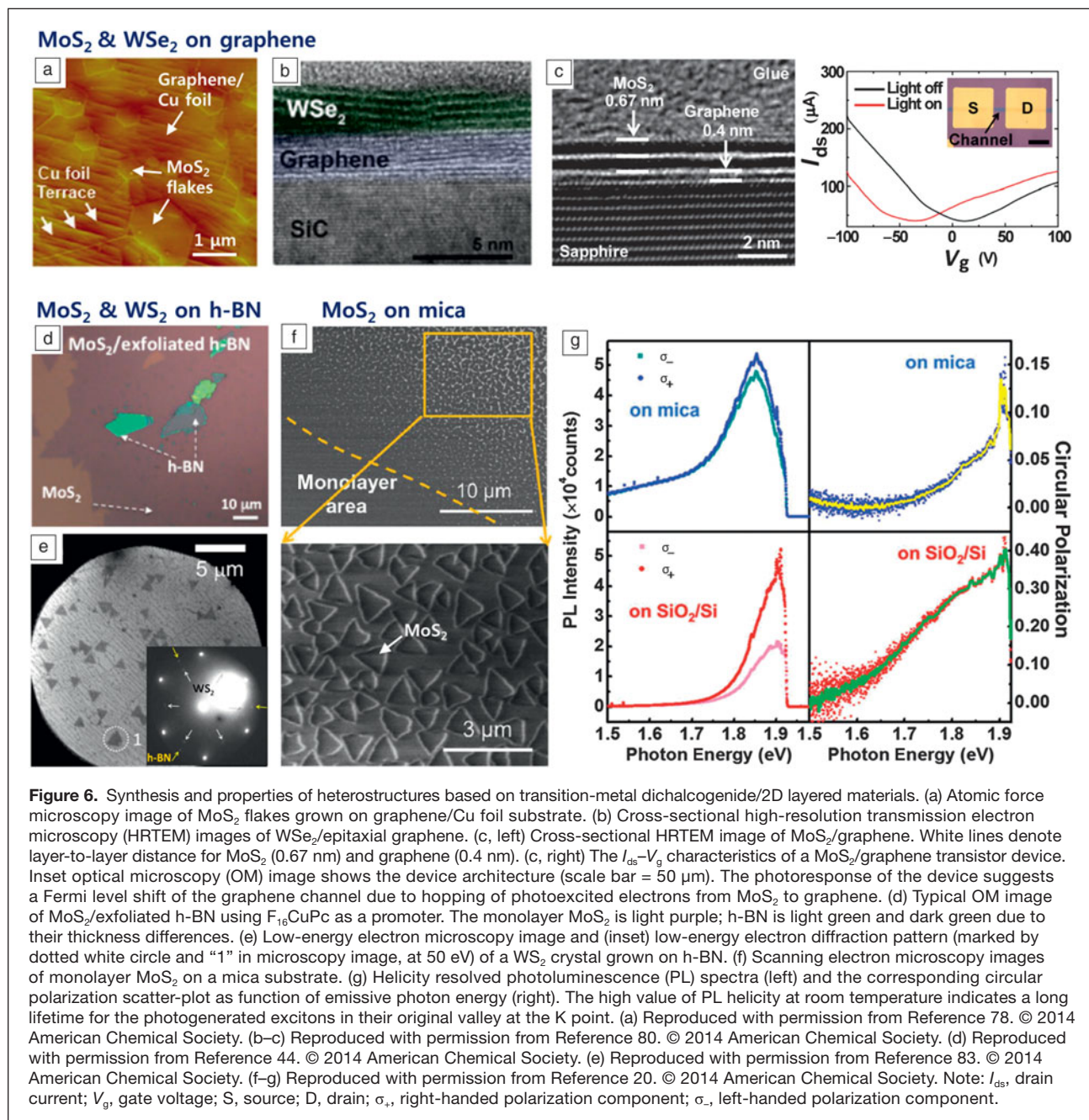
interlayer Type II excitons has been observed in artificially stacked MoS₂/WSe₂,^{69–71} WS₂/MoS₂,⁷² and WSe₂/MoSe₂⁷³ heterobilayers. **Figure 4** shows the PL spectra for an artificially stacked MoS₂/WSe₂ heterobilayer with interlayer coupling. Apart from the band edge PL from the MoS₂ (1.85 eV) and WSe₂ (1.67 eV), a Type II PL at 1.60 eV can be observed, indicative of interlayer coupling.

However, the fabrication of such artificial heterobilayers with the anticipated interlayer coupling remains challenging, since peel-and-paste processes would contaminate the hetero-interface, which could completely destroy the interlayer coupling and result in two independent monolayers. This problem can be partially resolved by post-fabrication annealing.^{70,72} **Figure 5** shows, in addition to the interlayer Type II PL emissions, the layer-number sensitive Raman out-of-plane mode A_{21g} for WSe₂ (309 cm⁻¹) and MoS₂ (463 cm⁻¹), as well as the appearance of the anomaly E'' mode for MoS₂ (286 cm⁻¹), which are also good indicators for the presence of interlayer coupling.⁷⁰

Compared to the approach based on artificial stacking, direct CVD growth is more promising for the mass production of various high-quality TMDC heterostructures with scalable size, controllable thickness, contamination-free interfaces, and reproducible electronic and optical properties. Remarkably, Gong et al. reported a scalable single-step vapor phase growth method for the formation of WS₂/MoS₂ heterostructures.²² By controlling the growth temperature, either vertically stacked or in-plane interconnected WS₂/MoS₂ heterostructures can be formed. At high growth temperatures, vertically stacked WS₂ layers on top of the MoS₂ monolayer with the preferred 2H stacking can

be formed. On the other hand, low temperature growth mostly results in lateral heterostructures of WS₂ on MoS₂ with atomically sharp heterojunctions.

Similar MoSe₂–WSe₂ lateral heterojunctions have also been fabricated by Huang et al. using the vapor–solid growth method.⁷⁴ Atomically resolved transmission electron microscopy (TEM) of the lateral heterostructure shows an undistorted lattice structure with substitution of one transition metal by another at the interface. Lateral heterostructures of the same transition metal but with different chalcogen atoms, such as MoS₂–MoSe₂ and WS₂–WSe₂, have also been realized by Duan and co-workers using *in situ* modulation of the chalcogenide vapor-phase reactants (sulfur/selenium) during growth.²³ Lateral heterojunctions can be formed epitaxially at the edges of existing TMDC domains. In particular, by combining *n*-type WS₂ and *p*-type WSe₂ laterally, monolayer *p*–*n*



diodes or even complementary metal oxide semiconductor inverters can be constructed.²³

For better control of the synthesis of either vertical or lateral TMDC heterostructures via CVD growth, independent and programmable control of chemical vapor sources of transition metals and chalcogens are desired. If such a CVD system becomes available, more sophisticated TMDC heterostructures, such as one-dimensional quantum wires, sandwiched 2D quantum wells, or vertical/lateral superlattices, can be realized by programmable control of the vapor sources as a function of time during growth. With rapid advances in the synthesis of novel TMDC heterostructures,

new device concepts and fascinating physics phenomena will emerge in the near future.

Synthesis and properties of heterostructures based on TMDC/other layer materials

Since h-BN has an atomically flat surface without dangling bonds or charged impurities,⁷⁵ it is expected that TMDC/h-BN heterostructures will show enhanced intrinsic properties such as high PL quantum yield and mobility compared to TMDCs on SiO₂.^{76,77} Recently, various approaches for the growth of TMDCs on graphene or h-BN templates have been tried. Kong et al. first reported, in 2012, a method for

epitaxial growth of MoS₂ on a graphene/Cu foil for a vertical heterostructure by low-pressure chemical vapor deposition (LPCVD) (Figure 6a).⁷⁸ They used (NH₄)₂MoS₄ dissolved in an organic solvent, *N,N*-DMF, as a precursor, which formed MoS₂ epitaxially on the graphene surface via thermal decomposition at low temperatures of 400°C. Even though there is relatively large lattice mismatch between MoS₂ and graphene (~28%),⁷⁹ the intrinsically weak vdW interaction between the two materials plays an important role in the formation of the MoS₂/graphene heterostructure, indicating that graphene can be a template for epitaxial growth of MoS₂.

Lin et al. also demonstrated the direct growth of MoS₂ or WSe₂ on epitaxial graphene on a SiC substrate, as shown in Figure 6b.^{80,81} Strain, wrinkling, and defects on the surface of graphene can be nucleation centers, and, in particular, MoS₂ on graphene can lead to a 10³ times improvement in photoresponse compared to MoS₂ alone, possibly due to the higher crystal quality of MoS₂ with an atomically sharp interface and the screening of the charge scattering from SiC by graphene. Subsequently, Lin et al. reported uniform MoS₂/graphene heterostructures on sapphire substrates.⁸² Sapphire was used to maximize the film size of the heterostructure and avoid possible chemical reactions between growth substrates. The number of MoS₂ layers were controlled by changing the amount of the precursor, MoCl₅. The cross-sectional high-resolution TEM image shown in Figure 6c (left) reveals direct evidence for a vertical heterostructure of MoS₂ and graphene with interlayer spacing of 0.67 nm and 0.4 nm, respectively. A Fermi level shift of the graphene channel on the MoS₂/graphene heterostructure was observed due to hopping of photoexcited electrons from MoS₂ to graphene (Figure 6c, right).

Kong et al. grew MoS₂ monolayers on mechanically exfoliated h-BN substrates using F₁₆CuPc as a seeding promoter, which was deposited on h-BN by thermal evaporation (Figure 6d).⁴⁴ Okada et al. reported the growth of WS₂ single layers on mechanically exfoliated h-BN using WC₁₆ and elemental sulfur as precursors by an atmospheric pressure CVD system.⁸³ The WS₂ grown on h-BN exhibited an intense sharp PL emission peak centered at 2.01 eV with a very small full width at half maximum of ~26 meV, indicating high-quality WS₂. Moreover, they measured low-energy electron diffraction patterns of WS₂/h-BN, shown in Figure 6e, indicating a distinct crystallographic relation between WS₂ and h-BN. This observation reveals the presence of substantial interaction between WS₂ and h-BN.

Similar to graphene and h-BN, fluorophlogopite mica (KMg₃AlSi₃O₁₀F₂) is also atomically flat and has a hexagonal crystalline structure with small lattice mismatch (~2.7%) with MoS₂. Thus, it is considered to be a good template for TMDC growth by CVD methods. Ji et al. reported that centimeter scale, single-layer MoS₂ could be grown on mica using LPCVD (Figure 6f).²⁰ They suggested that even a small lattice mismatch between mica and MoS₂ can induce intrinsic strain that quenches the PL. Figure 6g shows helicity-resolved PL spectra and corresponding circular polarization for MoS₂ on mica and on SiO₂/Si after transfer.²⁰ The complementary colored

curves inside the circular polarization scatter-plot are the adjacent-point-averaged results. The degree of circular polarization is defined as:

$$P(\sigma_+) = (I(\sigma_+) - I(\sigma_-)) / (I(\sigma_+) + I(\sigma_-)), \quad (1)$$

where $I(\sigma_+)$ and $I(\sigma_-)$ denote the PL intensity of the right- and left-handed components, respectively. MoS₂ on mica exhibited a low PL helicity, $P(\sigma_+)$, of less than 0.1, whereas MoS₂ transferred onto SiO₂/Si from mica showed a PL helicity of ~0.35 because of a dramatically decreased $I(\sigma_-)$ at room temperature. This phenomenon is due to the released strain of MoS₂ being transferred onto the SiO₂/Si substrate. The high PL helicity means a long lifetime for the photogenerated excitons, indicating high-quality MoS₂.

Summary

Semiconducting TMDC materials with tunable doping levels make them complementary to graphene and other 2D materials. Various methods have been developed for the synthesis of monolayer and few-layer TMDC nanosheets, among which the exfoliation method generates a range of well-dispersed TMDC monolayers in high-yield and large amounts, while chemical synthesis approaches can produce TMDC materials on the wafer-scale that are useful for the fabrication of electronic and optoelectronic devices. In addition, the electrodispersive properties and the semiconducting nature of TMDCs can be tailored by chemical doping and bandgap engineering. Novel properties and new phenomena also arise from 2D heterostructural stacking. To realize practical applications, more effort is required to address many issues related to the growth, including layer number control, size control, selective-area growth, and direct growth of heterostructures.

Acknowledgments

L.J.L. and Y.S. thank support from King Abdullah University of Science and Technology and the USA AFOSR BRI grant. W.H.C. and L.J.L. acknowledge support from the Center for Interdisciplinary Science of NCTU, Taiwan Consortium of Emergent Crystalline Materials (TCECM) and Ministry of Science and Technology, Taiwan (Grant No.: NSC102-2119-M-009-002-MY3). H.S.S. thanks support from the NRF grant (No. 20140610011) and a grant (CASE-2014M3A6A5060939) from the Center for Advanced Soft Electronics under the Global Frontier Research Program through the National Research Foundation funded by the Ministry of Science, ICT, and Future Planning, Korea. This work was supported by MOE under AcRF Tier 2 (ARC 26/13, No. MOE2013-T2-1-034), AcRF Tier 1 (RG 61/12, RGT18/13, and RG5/13), and Start-Up Grant (M4080865.070.706022), and Singapore Millennium Foundation in Singapore. Research was also conducted by NTU-HUJ-BGU Nanomaterials for the Energy and Water Management Programme under the Campus for Research Excellence and Technological Enterprise, which is supported by the National Research Foundation, Prime Minister's Office, Singapore.

References

- M. Chhowalla, H.S. Shin, G. Eda, L.-J. Li, K.P. Loh, H. Zhang, *Nat. Chem.* **5**, 263 (2013).
- X. Huang, Z. Zeng, H. Zhang, *Chem. Soc. Rev.* **42**, 1934 (2013).
- R. Ganatra, Q. Zhang, *ACS Nano* **8**, 4074 (2014).
- B. Radisavljevic, A. Radenovic, J. Brivio, V. Giacometti, A. Kis, *Nat. Nanotechnol.* **6**, 147 (2011).
- O. Lopez-Sanchez, D. Lembke, M. Kayci, A. Radenovic, A. Kis, *Nat. Nanotechnol.* **8**, 497 (2013).
- S. Bertolazzi, D. Krasnozhan, A. Kis, *ACS Nano* **7**, 3246 (2013).
- H. Wang, L. Yu, Y.-H. Lee, Y. Shi, A. Hsu, M.L. Chin, L.-J. Li, M. Dubey, J. Kong, T. Palacios, *Nano Lett.* **12**, 4674 (2012).
- Q. Ji, Y. Zhang, Y. Zhang, Z. Liu, *Chem. Soc. Rev.*, published online September 26, 2014, doi: 10.1039/C4CS00258J.
- Y. Shi, H. Li, L.-J. Li, *Chem. Soc. Rev.*, published online October 20, 2014, doi: 10.1039/C4CS00256C.
- T. Stephenson, Z. Li, B. Olsen, D. Mitlin, *Energy Environ. Sci.* **7**, 209 (2014).
- G. Eda, H. Yamaguchi, D. Voiry, T. Fujita, M. Chen, M. Chhowalla, *Nano Lett.* **11**, 5111 (2011).
- G. Eda, T. Fujita, H. Yamaguchi, D. Voiry, M. Chen, M. Chhowalla, *ACS Nano* **6**, 7311 (2012).
- X. Qian, J. Liu, L. Fu, J. Li, *Science* **346**, 1344 (2014).
- C. Lee, H. Yan, L.E. Brus, T.F. Heinz, J. Hone, S. Ryu, *ACS Nano* **4**, 2695 (2010).
- A. Splendiani, L. Sun, Y. Zhang, T. Li, J. Kim, C.-Y. Chim, G. Galli, F. Wang, *Nano Lett.* **10**, 1271 (2010).
- T.H. Ly, M.-H. Chiu, M.-Y. Li, J. Zhao, D.J. Perello, M.O. Cichocka, H.M. Oh, S.H. Chae, H.Y. Jeong, F. Yao, L.-J. Li, Y.H. Lee, *ACS Nano* **8**, 11401 (2014).
- W. Zhou, X. Zou, S. Najmaei, Z. Liu, Y. Shi, J. Kong, J. Lou, P.M. Ajayan, B.I. Yakobson, J.-C. Idrobo, *Nano Lett.* **13**, 2615 (2013).
- A.M. van der Zande, P.Y. Huang, D.A. Chenet, T.C. Berkelbach, Y. You, G.-H. Lee, T.F. Heinz, D.R. Reichman, D.A. Muller, J.C. Hone, *Nat. Mater.* **12**, 554 (2013).
- S. Najmaei, Z. Liu, W. Zhou, X. Zou, G. Shi, S. Lei, B.I. Yakobson, J.-C. Idrobo, P.M. Ajayan, *J. Lou, Nat. Mater.* **12**, 754 (2013).
- Q. Ji, Y. Zhang, T. Gao, Y. Zhang, D. Ma, M. Liu, Y. Chen, X. Qiao, P.-H. Tan, M. Kan, J. Feng, Q. Sun, Z. Liu, *Nano Lett.* **13**, 3870 (2013).
- X.-Q. Zhang, C.-H. Lin, Y.-W. Tseng, K.-H. Huang, Y.-H. Lee, *Nano Lett.* **15**, 410 (2014).
- Y. Gong, J. Lin, X. Wang, G. Shi, S. Lei, Z. Lin, X. Zou, G. Ye, R. Vajtai, B.I. Yakobson, H. Terrones, M. Terrones, B.K. Tay, J. Lou, S.T. Pantelides, Z. Liu, W. Zhou, P.M. Ajayan, *Nat. Mater.* **13**, 1135 (2014).
- X. Duan, C. Wang, J.C. Shaw, R. Cheng, Y. Chen, H. Li, X. Wu, Y. Tang, Q. Zhang, A. Pan, J. Jiang, R. Yu, Y. Huang, X. Duan, *Nat. Nanotechnol.* **9**, 1024 (2014).
- K.S. Novoselov, A.K. Geim, S.V. Morozov, D. Jiang, Y. Zhang, S.V. Dubonos, I.V. Grigorieva, A.A. Firsov, *Science* **306**, 666 (2004).
- K.S. Novoselov, D. Jiang, F. Schedin, T.J. Booth, V.V. Khotkevich, S.V. Morozov, A.K. Geim, *Proc. Natl. Acad. Sci. U.S.A.* **102**, 10451 (2005).
- H. Li, J. Wu, Z. Yin, H. Zhang, *Acc. Chem. Res.* **47**, 1067 (2014).
- H. Li, G. Lu, Y. Wang, Z. Yin, C. Cong, Q. He, L. Wang, F. Ding, T. Yu, H. Zhang, *Small* **9**, 1974 (2013).
- H. Li, G. Lu, Z. Yin, Q. He, H. Li, Q. Zhang, H. Zhang, *Small* **8**, 682 (2012).
- J.N. Coleman, M. Lotya, A. O'Neill, S.D. Bergin, P.J. King, U. Khan, K. Young, A. Gaucher, S. De, R.J. Smith, I.V. Shvets, S.K. Arora, G. Stanton, H.-Y. Kim, K. Lee, G.T. Kim, G.S. Duesberg, T. Hallam, J.J. Boland, J.J. Wang, J.F. Donegan, J.C. Grunlan, G. Moriarty, A. Shmeliov, R.J. Nicholls, J.M. Perkins, E.M. Grieveson, K. Theuwissen, D.W. McComb, P.D. Nellist, V. Nicolosi, *Science* **331**, 568 (2011).
- K.-G. Zhou, N.-N. Mao, H.-X. Wang, Y. Peng, H.-L. Zhang, *Angew. Chem. Int. Ed.* **50**, 10839 (2011).
- R.J. Smith, P.J. King, M. Lotya, C. Wirtz, U. Khan, S. De, A. O'Neill, G.S. Duesberg, J.C. Grunlan, G. Moriarty, J. Chen, J. Wang, A.I. Minett, V. Nicolosi, J.N. Coleman, *Adv. Mater.* **23**, 3944 (2011).
- V. Nicolosi, M. Chhowalla, M.G. Kanatzidis, M.S. Strano, J.N. Coleman, *Science* **340**, 1420 (2013).
- P. Joensen, R.F. Frindt, S.R. Morrison, *Mater. Res. Bull.* **21**, 457 (1986).
- M.B. Dines, *Mater. Res. Bull.* **10**, 287 (1975).
- E. Benavente, M.A. Santa Ana, F. Mendizábal, G. González, *Coord. Chem. Rev.* **224**, 87 (2002).
- H.S.S. Ramakrishna Matte, A. Gomathi, A.K. Manna, D.J. Late, R. Datta, S.K. Pati, C.N.R. Rao, *Angew. Chem. Int. Ed.* **49**, 4059 (2010).
- D. Voiry, H. Yamaguchi, J. Li, R. Silva, D.C.B. Alves, T. Fujita, M. Chen, T. Asefa, V.B. Shenoy, G. Eda, M. Chhowalla, *Nat. Mater.* **12**, 850 (2013).
- R. Kappera, D. Voiry, S.E. Yalcin, B. Branch, G. Gupta, A.D. Mohite, M. Chhowalla, *Nat. Mater.* **13**, 1128 (2014).
- Z. Zeng, Z. Yin, X. Huang, H. Li, Q. He, G. Lu, F. Boey, H. Zhang, *Angew. Chem. Int. Ed.* **50**, 11093 (2011).
- Z. Zeng, T. Sun, J. Zhu, X. Huang, Z. Yin, G. Lu, Z. Fan, Q. Yan, H.H. Hng, H. Zhang, *Angew. Chem. Int. Ed.* **51**, 9052 (2012).
- Z. Zeng, C. Tan, X. Huang, S. Bao, H. Zhang, *Energy Environ. Sci.* **7**, 797 (2014).
- K.-K. Liu, W. Zhang, Y.-H. Lee, Y.-C. Lin, M.-T. Chang, C.-Y. Su, C.-S. Chang, H. Li, Y. Shi, H. Zhang, *Nano Lett.* **12**, 1538 (2012).
- Y.-H. Lee, X.-Q. Zhang, W. Zhang, M.-T. Chang, C.-T. Lin, K.-D. Chang, Y.-C. Yu, J.T.-W. Wang, C.-S. Chang, L.-J. Li, T.-W. Lin, *Adv. Mater.* **24**, 2320 (2012).
- X. Ling, Y.-H. Lee, Y. Lin, W. Fang, L. Yu, M.S. Dresselhaus, J. Kong, *Nano Lett.* **14**, 464 (2014).
- S.M. Eichfeld, L. Hossain, Y.-C. Lin, A.F. Piasecki, B. Kupp, A.G. Birdwell, R.A. Burke, N. Lu, X. Peng, J. Li, A. Azcatl, S. McDonnell, R.M. Wallace, M.J. Kim, T.S. Mayer, J.M. Redwing, J.A. Robinson, *ACS Nano* **9**, 2080 (2015).
- S. McDonnell, R. Addou, C. Buie, R.M. Wallace, C.L. Hinkle, *ACS Nano* **8**, 2880 (2014).
- C.-H. Chen, C.-L. Wu, J. Pu, M.-H. Chiu, P. Kumar, T. Takenobu, L.-J. Li, *2D Mater.* **1**, 034001 (2014).
- Y. Shi, J.-K. Huang, L. Jin, Y.-T. Hsu, S.F. Yu, L.-J. Li, H.Y. Yang, *Sci. Rep.* **3**, 1839 (2013).
- Y. Shi, K.K. Kim, A. Reina, M. Hofmann, L.-J. Li, J. Kong, *ACS Nano* **4**, 2689 (2010).
- S. Mouri, Y. Miyauchi, K. Matsuda, *Nano Lett.* **13**, 5944 (2013).
- K. Dolui, I. Rungger, C. Das Pemmaraju, S. Sanvito, *Phys. Rev. B: Condens. Matter* **88**, 075420 (2013).
- J. Suh, T.-E. Park, D.-Y. Lin, D. Fu, J. Park, H.J. Jung, Y. Chen, C. Ko, C. Jang, Y. Sun, R. Sinclair, J. Chang, S. Tongay, J. Wu, *Nano Lett.* **14**, 6976 (2014).
- H. Li, X. Duan, X. Wu, X. Zhuang, H. Zhou, Q. Zhang, X. Zhu, W. Hu, P. Ren, P. Guo, L. Ma, X. Fan, X. Wang, J. Xu, A. Pan, X. Duan, *J. Am. Chem. Soc.* **136**, 3756 (2014).
- Y. Gong, Z. Liu, A.R. Lupini, G. Shi, J. Lin, S. Najmaei, Z. Lin, A.L. Elías, A. Berkdemir, G. You, H. Terrones, M. Terrones, R. Vajtai, S.T. Pantelides, S.J. Pennycook, J. Lou, W. Zhou, P.M. Ajayan, *Nano Lett.* **14**, 442 (2013).
- S.-H. Su, W.-T. Hsu, C.-L. Hsu, C.-H. Chen, M.-H. Chiu, Y.-C. Lin, W.-H. Chang, K. Suenaga, J.-H. He, L.-J. Li, *Front. Energy Res.* **2**, 27 (2014).
- B. Li, L. Huang, M. Zhong, N. Huo, Y. Li, S. Yang, C. Fan, J. Yang, W. Hu, Z. Wei, J. Li, *ACS Nano* **9**, 1257 (2015).
- A.K. Geim, I.V. Grigorieva, *Nature* **499**, 419 (2013).
- L. Britnell, R.M. Ribeiro, A. Eckmann, R. Jalil, B.D. Belle, A. Mishchenko, Y.-J. Kim, R.V. Gorbachev, T. Georgiou, S.V. Morozov, A.N. Grigorenko, A.K. Geim, C. Casiraghi, A.H.C. Neto, K.S. Novoselov, *Science* **340**, 1311 (2013).
- M.-L. Tsai, S.-H. Su, J.-K. Chang, D.-S. Tsai, C.-H. Chen, C.-I. Wu, L.-J. Li, L.-J. Chen, J.-H. He, *ACS Nano* **8**, 8317 (2014).
- L. Britnell, R.V. Gorbachev, R. Jalil, B.D. Belle, F. Schedin, A. Mishchenko, T. Georgiou, M.I. Katsnelson, L. Eaves, S.V. Morozov, N.M.R. Peres, J. Leist, A.K. Geim, K.S. Novoselov, L.A. Ponomarenko, *Science* **335**, 947 (2012).
- P.T.K. Loan, W. Zhang, C.-T. Lin, K.-H. Wei, L.-J. Li, C.-H. Chen, *Adv. Mater.* **26**, 4838 (2014).
- Y.-H. Chang, F.-Y. Wu, T.-Y. Chen, C.-L. Hsu, C.-H. Chen, F. Wiryo, K.-H. Wei, C.-Y. Chiang, L.-J. Li, *Small* **10**, 895 (2014).
- A.J. Smith, Y.-H. Chang, K. Raidongia, T.-Y. Chen, L.-J. Li, J. Huang, *Adv. Energy Mater.* **4**, 1400398 (2014).
- Y. Shi, Y. Wang, J.I. Wong, A.Y.S. Tan, C.-L. Hsu, L.-J. Li, Y.-C. Lu, H.Y. Yang, *Sci. Rep.* **3**, 2169 (2013).
- X. Cao, Y. Shi, W. Shi, X. Rui, Q. Yan, J. Kong, H. Zhang, *Small* **9**, 3433 (2013).
- J. Kang, S. Tongay, J. Zhou, J. Li, J. Wu, *Appl. Phys. Lett.* **102**, 012111 (2013).
- C. Gong, H. Zhang, W. Wang, L. Colombo, R.M. Wallace, K. Cho, *Appl. Phys. Lett.* **103**, 053513 (2013).
- H. Terrones, F. López-Urías, M. Terrones, *Sci. Rep.* **3**, 1549 (2013).
- H. Fang, C. Battaglia, C. Carraro, S. Nemsak, B. Ozdol, J.S. Kang, H.A. Bechtel, S.B. Desai, F. Kronast, A.A. Unal, G. Conti, C. Conlon, G.K. Palsson, M.C. Martin, A.M. Minor, C.S. Fadley, E. Yablonovitch, R. Maboudian, A. Javey, *Proc. Natl. Acad. Sci. U.S.A.* **111**, 6198 (2014).
- M.-H. Chiu, M.-Y. Li, W. Zhang, W.-T. Hsu, W.-H. Chang, M. Terrones, H. Terrones, L.-J. Li, *ACS Nano* **8**, 9649 (2014).
- C.-H. Lee, G.-H. Lee, A.M. van der Zande, W. Chen, Y. Li, M. Han, X. Cui, G. Arefe, C. Nuckolls, T.F. Heinz, J. Guo, J. Hone, P. Kim, *Nat. Nanotechnol.* **9**, 676 (2014).
- S. Tongay, W. Fan, J. Kang, J. Park, U. Koldemir, J. Suh, D.S. Narang, K. Liu, J. Ji, J. Li, R. Sinclair, J. Wu, *Nano Lett.* **14**, 3185 (2014).
- P. Rivera, J.R. Schaibley, A.M. Jones, J.S. Ross, S. Wu, G. Aivazian, P. Klement, K. Seyler, G. Clark, N.J. Ghimire, J. Yan, D.G. Mandrus, W. Yao, X. Xu, *Nat. Commun.* **6**, 6242 (2015).
- C. Huang, S. Wu, A.M. Sanchez, J.J.P. Peters, R. Beanland, J.S. Ross, P. Rivera, W. Yao, D.H. Cobden, X. Xu, *Nat. Mater.* **13**, 1096 (2014).
- Y. Shi, C. Hamsen, X. Jia, K.K. Kim, A. Reina, M. Hofmann, A.L. Hsu, K. Zhang, H. Li, Z.-Y. Juang, M.S. Dresselhaus, L.-J. Li, J. Kong, *Nano Lett.* **10**, 4134 (2010).
- K.F. Mak, K. He, J. Shan, T.F. Heinz, *Nat. Nanotechnol.* **7**, 494 (2012).

77. G.-H. Lee, Y.-J. Yu, X. Cui, N. Petrone, C.-H. Lee, M.S. Choi, D.-Y. Lee, C. Lee, W.J. Yoo, K. Watanabe, T. Taniguchi, C. Nuckolls, P. Kim, J. Hone, *ACS Nano* **7**, 7931 (2013).

78. Y. Shi, W. Zhou, A.-Y. Lu, W. Fang, Y.-H. Lee, A.L. Hsu, S.M. Kim, K.K. Kim, H.Y. Yang, L.-J. Li, J.-C. Idrobo, J. Kong, *Nano Lett.* **12**, 2784 (2012).

79. Y. Ma, Y. Dai, M. Guo, C. Niu, B. Huang, *Nanoscale* **3**, 3883 (2011).

80. Y.-C. Lin, N. Lu, N. Perea-Lopez, J. Li, Z. Lin, X. Peng, C.H. Lee, C. Sun, L. Calderin, P.N. Browning, M.S. Bresnehan, M.J. Kim, T.S. Mayer, M. Terrones, J.A. Robinson, *ACS Nano* **8**, 3715 (2014).

81. Y.-C. Lin, C.-Y.S. Chang, R.K. Ghosh, J. Li, H. Zhu, R. Addou, B. Diaconescu, T. Ohta, X. Peng, N. Lu, M.J. Kim, J.T. Robinson, R.M. Wallace, T.S. Mayer, S. Datta, L.-J. Li, J.A. Robinson, *Nano Lett.* **14**, 6936 (2014).

82. M.-Y. Lin, C.-E. Chang, C.-H. Wang, C.-F. Su, C. Chen, S.-C. Lee, S.-Y. Lin, *Appl. Phys. Lett.* **105**, 073501 (2014).

83. M. Okada, T. Sawazaki, K. Watanabe, T. Taniguchi, H. Hibino, H. Shinohara, R. Kitaura, *ACS Nano* **8**, 8273 (2014).

84. J. Zheng, H. Zhang, S. Dong, Y. Liu, C.T. Nai, H.S. Shin, H.Y. Jeong, B. Liu, K.P. Loh, *Nat. Commun.* **5**, 2995 (2014). □

THE 2015
MRS SPRING
MEETING
ON DEMAND

MRS OnDemand® NEW CONTENT AVAILABLE NOW!

The 2015 MRS Spring Meeting was one of our best yet, and now, with MRS OnDemand, you can view select talks and lectures from the Meeting, complete with presentation materials, from the comfort of your home or office, or on the go!

▶ FEATURED EVENTS

Fred Kavli Distinguished Lectureship in Nanoscience

Hongyou Fan, Sandia National Laboratories and The University of New Mexico
Nanomaterials under Stress—A New Opportunity for Nanomaterials Synthesis and Engineering

Symposium X—Frontiers of Materials Research

Alexandra Navrotsky, University of California, Davis
Energetics at the Nanoscale—Impacts for Geochemistry, the Environment and Materials

Lionel Vayssieres, International Research Center for Renewable Energy
Advanced Low Cost Energy Materials from Aqueous Solutions

Daniël Vanmaekelbergh, Debye Institute for Nanomaterials Science, University of Utrecht
Colloidal Nanocrystals: From Individual Quantum Objects to Building Blocks for Honeycomb Semi-conductors Hosting Dirac Carriers

▶ TUTORIAL SESSIONS

Tutorial P

Nanogenerators and Piezotronics—From Working Principles to Applications

Tutorial Y

Overview of Phase-Change Materials, Their Physics and Applications

Tutorial CC

Reliability and Materials Issues of Semiconductor Optical and Electron Devices and Materials

Tutorial OO

Introduction to Metal-Assisted Chemical Etching—Chemistry and Applications

Tutorial WW

Measure Ultrafast Dynamics—How and Why

▶ SELECT TALKS FROM 12 TECHNICAL SESSIONS

▶ AWARDS OF THE MATERIALS RESEARCH SOCIETY

Mid-Career Researcher Award

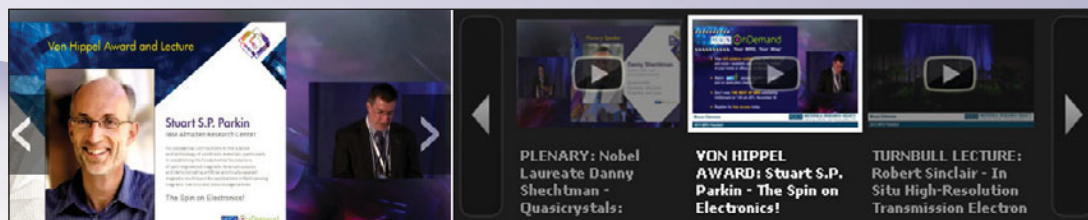
Seth R. Marder, Georgia Institute of Technology
The Design of Organic Molecules and Materials for Nonlinear Optical Applications

Innovation in Materials Characterization Award

John M. Carpenter, Argonne National Laboratory
History, Development and Applications of Neutron Sources

Outstanding Young Investigator Award

Karena W. Chapman, Argonne National Laboratory
Accelerating the Development of Energy Materials Through Advanced X-ray Tools



IT'S YOUR MRS, YOUR WAY!

www.mrs.org/on-demand